

# Is the pinning of ordinary dislocations in $\gamma$ -TiAl intrinsic or extrinsic in nature? A combined atomistic and kinetic Monte Carlo approach

I.H. Katzarov\*, A.T. Paxton

*Atomistic Simulation Centre, School of Mathematics and Physics, Queen's University Belfast, Belfast BT7 1NN, UK*

Received 28 June 2010; received in revised form 25 October 2010; accepted 27 October 2010

Available online 2 December 2010

## Abstract

We address the question of the observed pinning of  $\frac{1}{2}\langle 1\bar{1}0 \rangle$  ordinary screw dislocations in  $\gamma$ -TiAl, which leads to the characteristic trailing of dipoles in the microstructure. While it has been proposed that these may be variously intrinsic or extrinsic in nature, we are able to rule out the former mechanism. We do this by means of very large scale, three-dimensional atomistic simulations using the quantum mechanical bond order potential. We find that the kink-pair formation energy is large – 6 eV – while the single kink migration energy is conversely very small – 0.13 eV. Using these, and other atomistically derived, data, we make kinetic Monte Carlo simulations at realistic time and length scales to simulate dislocation mobility as a function of stress and temperature. In the temperature range of the stress anomaly in  $\gamma$ -TiAl, we determine whether one or several of the pinning and unzipping processes associated with generation of jogs are observed during our simulations. We conclude that the pinning of ordinary dislocations and anomalous mechanical behaviour in  $\gamma$ -TiAl must be attributed to a combination of extrinsic obstacles and extensive cross-slip in a crystal containing impurities. © 2010 Acta Materialia Inc. Published by Elsevier Ltd. All rights reserved.

**Keywords:** Modelling; Dislocation mobility; Monte Carlo techniques; Titanium alloys

## 1. Introduction

It is well known that the deformation behaviour of  $\gamma$ -TiAl is complex due to the tetragonality of the  $L1_0$  structure. The  $\gamma$  phase of TiAl can deform by several deformation modes: glide of ordinary dislocations, glide of superlattice dislocations and twinning [1]. The  $\mathbf{b} = \frac{1}{2}\langle 1\bar{1}0 \rangle$  ordinary dislocations in deformed TiAl alloys exhibit a unique morphology consisting of numerous pinning points along the dislocation line aligned roughly along the screw dislocation direction, and bowed-out segments between the pinning points [1]. Post mortem TEM analyses [2–4] have shown that the screw segments separated by pinning points are lying in different parallel (111) planes as a result of a cross-slip mechanism. Extensive cross-slip was also observed in in situ straining experiments [5]. Yield stress anomaly (increase of the yield

stress with temperature) has been observed in  $\gamma$ -TiAl compounds and ascribed to the  $\frac{1}{2}\langle 1\bar{1}0 \rangle\{111\}$  slip system [3,6,7]. There is compelling microscopic evidence that pinning plays a prominent role in the anomalous mechanical behaviour. The determination of the subsequent cusp unpinning mechanism is of fundamental importance in the interpretation of the stress anomaly.

Deep cusps and the trailing of dipoles suggest that the dislocations have many jogs. At the microscopic scale, the pinning points have been analysed as jogs aligned along the screw direction, whose density increases with temperature in the domain of the stress anomaly [8,9]. The exact nature of the obstacles developed on these cross-kinks seems to be controversial. Viguier et al. [3] and Sriram et al. [4] have concluded that the pinning points are formed as a result of intrinsic processes involving single or double cross-slip mechanisms, leading to formation of jogs. The three-dimensional (3-D) structure formed during collision of kinks during their lateral propagation cannot move in the direction of the dislocation glide. Explanations based

\* Corresponding author. Tel.: +44 (0) 28 9097 1425; fax: +44 (0) 28 9097 3110.

E-mail address: [i.katzarov@qub.ac.uk](mailto:i.katzarov@qub.ac.uk) (I.H. Katzarov).

on the activation of cross-slip suffer, however, from not explaining satisfactorily a number of experimental results:

1. Non-screw ordinary dislocations, Shockley dislocations involved in twinning and superlattice dislocations are also anchored at many points [10–13].
2. Ordinary dislocations moving in the same plane are able to anchor at exactly the same location in the sample [5].
3. An annealing treatment which precipitates interstitial atoms in excess decreases the density of cusps and debris [2].

To explain these experimental results, it was concluded that pinning points are extrinsic in nature and due to some chemical heterogeneity [2,11,14]. Messerschmidt et al. [10] and Morris [15] have ascribed these pinning points to small extrinsic obstacles like oxygen atoms or  $\text{Al}_2\text{O}_3$  precipitates.

Understanding the glide mechanism of ordinary dislocations in different stress and temperature ranges can help us to determine which of its main features is likely to account for the strength anomaly of  $\gamma$ -TiAl. In addition, the behaviour of these ordinary dislocations deserves particular attention since they are responsible for most of the deformation in two-phase lamellar TiAl alloys [16–19].

The present work aims at exploring the mobility of  $\frac{1}{2}\langle 1\bar{1}0 \rangle$  ordinary screw dislocations in  $\gamma$ -TiAl through simulation of the specific mechanisms of motion of an individual dislocation in the  $L1_0$  structure.

Due to the high Peierls barrier [16,20], the motion of ordinary screw dislocations in TiAl is believed to be controlled by nucleation, migration and annihilation of kinks. When the stress on a dislocation is lower than its Peierls stress, the dislocation line stays at rest in a given lattice position, interrupted by the thermally assisted process of kink-pair nucleation. The separation of kinks under the influence of stress and thermal activation results in translation of the entire dislocation line to the next lattice position. The overall dislocation movement is a cumulative effect of a large number of individual kink events.

Dislocation dynamics (DD) simulations [21,22] employ simple rules that dictate the motions of dislocations which are represented as interconnected small straight segments in an elastic continuum connected through nodes. Local stresses resulting from applied loading and internal stresses are computed on each of those segments. The dynamics of dislocation motion is thus reduced to the dynamics of the nodes prescribed by the mobility rules. Such a description replaces the true kink dynamics of dislocation glide with a mean field measure of the average mobility of a dislocation line. The reliability with which the DD simulations mimic the plastic behaviour of the crystal depends on the accuracy of the mobility rules.

In order to overcome these limitations and to obtain a more realistic description of the dynamics of a dislocation line over long time scales, we carry out kinetic Monte Carlo (kMC) simulations of the mobility of  $\frac{1}{2}\langle 1\bar{1}0 \rangle$  dislocations. Several researchers have performed kMC studies of dislo-

cation behaviour to provide a more realistic link between kink dynamics and the averaged dynamics of a dislocation line [23–25]. The advantage of this approach is that it replaces arbitrary assumptions about the nature of dislocation mobility with input based upon microscopic understanding. In addition, kMC can achieve extended time scales for simulation of the dislocation mobility. kMC simulations use atomistic results for the nature of the core energetics, short-range dislocation segment interactions and rate theory to simulate dislocation mobility as a function of stress and temperature.

In our simulations we assume that the ordinary dislocation moves by the kink mechanism through adjacent Peierls valleys. We examine ordinary dislocation mobility in TiAl at fixed stresses and temperatures based upon atomistic input. The rates of kink-pair nucleation and kink migration events are expressed in terms of their respective energy barriers, which are computed using atomistic simulation techniques. The kMC model allows dislocations to cross-slip onto secondary glide planes. Thus, motion of screw dislocations becomes three-dimensional and can involve a number of unusual mechanisms affecting dislocation mobility. In the temperature range of the stress anomaly, we check whether one or several of the above-mentioned pinning and unzipping processes associated with generation of jogs are observed during simulations.

## 2. kMC model

Ordinary screw dislocations in TiAl do not dissociate into a planar structure due to the high energy of the complex stacking fault (CSF) in  $\gamma$ -TiAl [20]. Instead, the non-planar core of these dislocations spreads symmetrically on two cross-slip  $\{111\}$  planes (Fig. 1) and their glide is not confined to a single glide plane. Cross-slip should readily occur by which screw dislocations change their glide planes. In fact, each screw dislocation segment can nucleate kink-pairs on either of the two  $\{111\}$  planes.

The kMC model does not consider any details of the core structure. It focuses on dislocation motion on length and time scales far greater than those of atomistic simulations. The key idea of kMC is to treat dislocation motion as a stochastic sequence of discrete rare events whose mechanisms and rates are computed within the framework of transition state theory. Dislocations are represented as interconnected small straight segments in an elastic continuum. Local stresses resulting from applied loading and internal stresses are computed on each of those segments.

In the present model, we study the ordinary screw dislocation represented by a piecewise straight line stretched along the  $[1\bar{1}0]$  direction. While the dislocation has, on average, a screw orientation, it consists of screw (S) and edge (E) dislocation segments such that kinks on the screw dislocation are perfect edge segments. E-segments all have the same length  $h$ , the unit kink height, while S-segments can be of any length. In the present work we choose for the length of the smallest S-segment  $a = b$ , where  $\mathbf{b} = \frac{1}{2}\langle 1\bar{1}0 \rangle$  is the

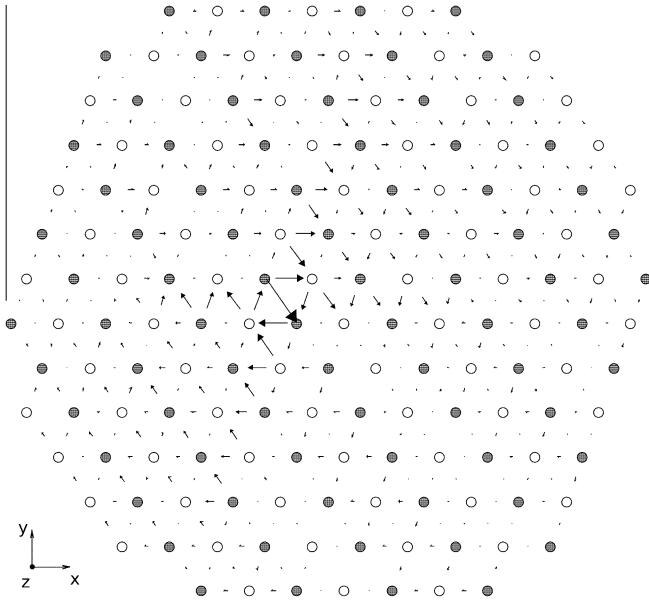


Fig. 1. Differential displacement plot showing the screw components of a  $\frac{1}{2}[1\bar{1}0]$  screw dislocation. The arrows joining atom pairs indicate the relative displacements of the two atoms in the direction normal to the page; hence the arrows show the screw component of the relative displacement. The length of the arrow (in arbitrary units) is proportional to the amount of relative displacement.

Burgers vector of the screw dislocation. The time and 3-D space is discretized in the form of a square grid. Here,  $a$  and  $h$  are the grid spacings in the screw and edge directions, respectively.

The screw dislocation in TiAl was allowed to move on the two  $\{111\}$  glide planes that comprise the  $\frac{1}{2}(1\bar{1}0)\{111\}$  slip system. Kink-pairs are allowed to nucleate on any part of S-segments and in any of the two  $\{111\}$  glide planes intersecting the  $[1\bar{1}0]$  direction. Once nucleated, a kink (E-segment) can move in its glide plane along the dislocation line until it recombines with another kink with the opposite sign. Periodic boundary conditions are applied so that kinks leaving at one end re-enter the dislocation from the other end. During kMC simulations, the dislocation moves under the action of external stress through kink-pair nucleation, migration and recombination. This model does not allow for climb of the edge segments.

The kMC simulation samples different classes of possible kink nucleation and migration events. Kink-kink annihilation is considered as a special case of kink migration. The kMC methods use information on the energetic barriers to atomic hopping or kink migration that control the motion of a dislocation in order to obtain the relationships between the velocity of the dislocation and the driving forces acting upon it. The kinetics of dislocation motion is completely specified by the matrix of transition rates. Transition-state theory expresses the rates of kink-pair nucleation and kink migration events in terms of their respective energy barriers, which can be computed using atomistic simulations. The following form of transition-rate matrix element provides a physically consistent

description of the energetics and thermally activated formation of kink-pairs [27]:

$$J_{k-p}(n) = \omega \exp \left[ -\frac{\Delta E_n - TS - \sigma_{\text{eff}} b \Delta A(n)/2}{k_B T} \right]$$

$\Delta E_n$  is the formation energy of a kink-pair,  $k_B$  is the Boltzmann constant and  $\omega$  is the pre-exponential “frequency” factor, which is set equal to the Debye frequency.  $\sigma_{\text{eff}}$  is the local resolved stress that includes the applied stress and the self-stress field. The self-stress is the stress exerted on a dislocation segment by all other dislocation segments and can be calculated from the gradient of the total energy of the dislocation configuration due to virtual displacements of the segment [27]. The total energy is computed by using non-singular continuum theory of dislocations [28]. The major advantage of this theory is that it contains no singularities. The singularity intrinsic to the classical continuum theory is removed by spreading the Burgers vector isotropically about every point on the dislocation line using a spreading function characterized by a single parameter  $r_c$ , the spreading radius. The non-singular expression for dislocation energy depends on the choice of the cut-off parameter  $r_c$ . We determined it by comparing the energy of a kink-pair predicted by non-singular continuum theory with atomistic data.  $S$  is usually taken to be  $3k_B$  [27]. The last term is the work done by the external applied stress and  $\Delta A(n)$  is the change of the area of the glide plane as a result of kink-pair formation.

A kink, once formed, can migrate along the dislocation line. The rate of migration of the kinks depends on the magnitude of the activation energy for kink motion  $W_n$  (secondary Peierls barrier). If this is very large, the kink migration is thermally activated, with the transition rate given by

$$J_m = \omega \exp \left[ -\frac{W_n - TS - \sigma_{\text{eff}} b^2 h/2}{k_B T} \right] \quad (1)$$

If the secondary Peierls barrier for the kink motion is very small, the kink migration is not thermally activated but is controlled by phonon drag. In such a case, the kink velocity  $v_k$  is proportional to the driving force experienced by the kink. In the kMC model the thermally activated migration events specified by the transition rates (1) are replaced by continuous movement of the kinks with velocity proportional to the stress of the dislocation line calculated at that instant [25,26].

### 2.1. Sustainable kink-pair nucleation

The dislocations in the kMC model are discretized as sets of screw and edge segments. Our atomistic simulations, described in the following section, predict that a screw segment of the dislocation line moves to an adjacent Peierls valley upon nucleation of kink-pair only if the distance between the kinks is greater than the kink width  $w_c = 16b$ . Only in this case can the kink-pair be represented by a set of screw and edge segments with length  $h$ . If a kink-pair is formed with a width smaller than a critical width  $w_c$ , the height of the kinks

is smaller than the grid spacing in the edge direction. In this case the kink-pair cannot be represented by a continuous piecewise straight line on the discretized space. In addition, the elastic energy of such configurations cannot be calculated accurately by using non-singular continuum theory of dislocations. A solution to this problem lies in nucleating a kink-pair only of finite width  $w_{in}$  that is greater than the critical width  $w_c$ . Such a kink-pair, once formed, can be represented by a continuous piecewise straight line on the discretized space and its elastic energy can be calculated correctly. To be able to do that, it is necessary to compute the rate at which such kink-pairs should be nucleated. We determine the rate for the formation of a kink-pair of width  $w > w_c$  by using survival probabilities analysis on the 1-D random walk. Details of this method can be found elsewhere [29,30].

The survival probability  $p(1 \rightarrow n)$ , which is defined as the probability that a kink-pair of width  $w = 1b$  expands to  $w = nb$  before it shrinks to  $w = 0$ , can be obtained from

$$p(1 \rightarrow n) = \prod_{k=1}^n p(k \rightarrow k+1)$$

and  $p(k \rightarrow k+1)$  can be calculated from the following recursive formulae:

$$p(k \rightarrow k+1) = \frac{F(k)}{1 - [1 - F(k)]p(k-1 \rightarrow k)}$$

$F(k) = J^+(k)/J^-(k)$  is the probability that upon escape from state  $kb$  the kink-pair will expand to width  $(k+1)b$ .  $J^+(k)$  and  $J^-(k)$  are the rates of forward and backward jumps from state  $k$  as follows:

$$J^+(k) = \omega \exp\left(-\frac{[E(k+1) - E(k)] - TS - \sigma_{eff} b \Delta A(k)/2}{k_B T}\right) [1 + H(k)] \quad (2)$$

$$J^-(k) = \omega \exp\left(-\frac{[E(k-1) - E(k)] - TS - \sigma_{eff} b \Delta A(k)/2}{k_B T}\right) [1 + H(k-1)] \quad (3)$$

where  $H(k) = 1$  if  $k \geq 1$  and  $H(k) = 0$  if  $k \leq 0$ . With this definition the rate of embryonic kink-pair nucleation is simply  $J(1) = J^+(0)$ .  $E(k)$  is the energy of two kinks separated by a distance  $kb$ . The approximation we employ here by describing the rates of forward and backward jumps in the forms (2) and (3) is that the local stress remains constant over the time it takes for an embryonic kink-pair to expand to width  $nb$ . This approximation is fairly good because, under the conditions considered here, the expansion time is usually very small compared to the time over which the dislocation configuration and the local stresses change significantly. When the distance between the kinks  $kb$  is smaller than the critical width  $w_c$ ,  $E(k)$  is specified by the kink-pair formation energy, which is calculated atomistically (Section 3.2, Fig. 4, below). The rate at which kink-pairs of width  $w_{in}b$  greater than the critical width  $w_c$  appear can be obtained from the rate of embryonic kink-pair nucleation  $J(1)$  and the corresponding survival probability

$$J(n) = J(1)p(1 \rightarrow n) \quad (4)$$

In our kMC model only kink-pairs with width  $w_{in} > w_c$  are allowed to nucleate on S-segments with appropriate length  $L_S > w_c$ . The nucleation rate of such kink-pairs is given by (4).

### 3. Atomistic simulations

A crucial input for kMC simulations is the information from atomistic simulations of the properties of dislocation cores and short-range dislocation segment-segment interactions, such as the energies of a single isolated and kink-pair and the associated Peierls stress for kink motion. As both the qualitative and quantitative outcome of the kMC simulations is extremely sensitive to these input quantities, the accuracy of the atomistic simulations is of utmost importance.

The atomistic simulation of individual dislocations requires special treatment due to the long-ranged elastic field associated with them. For long straight dislocations, we may use a periodicity along the dislocation line, but should avoid using periodic boundary conditions in the other two directions since the dislocation strain field is very long ranged. The cells used in these simulations, as in most real space calculations, are divided into two regions of relaxing and non-relaxing atoms, the latter bounded by a free surface sufficiently far from the core to avoid image stresses.

Pettifor's bond order potential (BOP) [31,32] represents a numerically efficient scheme that works within the orthogonal tight binding approximation with environment dependent matrix elements. The multi-atom character of the forces, is thereby captured in a physical way that goes beyond the standard pair functionals (Finnis–Sinclair or embedded atom method). Apart from their genuine quantum-mechanical origin, BOPs have two additional important advantages. First, the evaluation of the energy scales linearly in computational time with the number of atoms, and second, the real-space formalism avoids the need of imposing full periodic boundary conditions common to  $k$ -space methods. Both of these features are crucial for studies of dislocations since such simulations often require a large number of atoms and complex geometries. The atomistic simulations of the the properties of ordinary screw dislocations in this study have been made using the BOP for  $\gamma$ -TiAl, constructed and extensively tested against accurate first-principles methods [33].

Molecular statics (MS) techniques, which seek to minimize the total energy of the system at zero-temperature, can be used for relaxation of the inner atomistic regions of the simulation cell, where the initial atomic positions in the computational cell are established by the conditions of linear anisotropic elasticity. Traditionally, fixed boundary conditions have been most often used in such dislocation simulations. This requires very large simulation cells in practice, but this method is always problematic with respect to force build-up between fixed and relaxed atomic regions. The size of the atomistic region can be dramatically reduced

by using so-called flexible boundary conditions. An elastic Green's function version of such conditions have been developed for both 2-D and 3-D dislocation simulations, known as Green's function boundary conditions (GFBC) [34,35]. The GF techniques allow dislocation configurations to be simulated atomistically with very little accumulation of forces at the boundaries of the simulation cells. In this method, a buffer layer is introduced between the fixed outer and inner relaxed atomistic regions of the simulation cell, allowing one to dynamically update the boundary conditions of the simulation, while dramatically reducing the size of the atomistic region.

Using the BOP method for the description of the interatomic interactions, we have implemented GFBC to calculate the properties of ordinary screw dislocations through MS simulations. These properties include the core structure and energy, the kink-pair formation energy, the primary and secondary Peierls stresses as well as the kink motion activation energies. In this way, the simulated 3-D dislocation configurations can be contained in significantly reduced atomistic region without compromising the fidelity of the final core structure and energy.

### 3.1. Isolated kink

Two 2-D core structures of an infinite  $\frac{1}{2}[1\bar{1}0]$  screw dislocation were used to obtain the initial approximation to the structure of a kink. These relaxed configurations of the 2-D ordinary screw dislocation were constructed by using two different elastic centres in an initial approximation to the dislocation displacement field. Anisotropic elasticity theory was used to introduce a  $\frac{1}{2}[1\bar{1}0]$  screw dislocation in the simulation cell. A cylindrical crystal, one periodic unit in length along the dislocation line direction,  $[1\bar{1}0]$ , was constructed in order to obtain the two symmetry-related core structures of the ordinary screw dislocation. The  $x$  and  $y$  axes in the simulation cell were  $[11\bar{2}]$  and  $[111]$  respectively. The centres of the two core structures were introduced at two adjacent Peierls valleys with a relative displacement of  $h$ , the periodic length along the  $[11\bar{2}]$  direction. Atomistic relaxation was used to optimize the atomic positions in the active region. The 2-D GF procedure was applied to relieve the boundary forces. One of the relaxed configurations obtained for the core structure of straight  $\frac{1}{2}[1\bar{1}0]$  screw dislocations is shown in a differential displacement plot in Fig. 1.

The two 2-D cores are then used to obtain the initial approximation to the structure of an isolated kink on an ordinary screw dislocation. A 3-D cylindrical cell is constructed with a total length of  $45b$ , where  $b$  is the Burgers vector of the dislocation. The two halves of the simulation cell were made up of 22 periodic units of the two relaxed configurations of the 2-D  $\frac{1}{2}[1\bar{1}0]$  screw dislocation respectively. The central cell of unit length  $b$  was defined as the average of the positions of identical atoms in the two 2-D core structures [35]. This overall length  $45b$  is chosen to allow a smooth transition from one core structure to

the next. Using a simple continuum estimate of the width of the kink [35,36], we obtain a kink width of  $13b$ . Therefore  $45b$  is a reasonable choice for the overall length of the simulation cell.

Relaxation is carried out in the inner atomistic region and the GF technique is used to relax the forces that develop in the buffer GF layer. The core structure of the central cell of the kinked dislocation line was characterized using differential displacement plots (Fig. 2). The difference between the energies of the kinked and straight dislocation gives the single-kink formation energy. The formation energy of an isolated kink in  $\gamma$ -TiAl calculated by our atomistic simulations is 2.88 eV.

In order to determine the width of the kink, we plot the differences  $\Delta z = [z_3 + z_4 - (z_1 + z_2)]/2$  between the average  $z$ -coordinates of the atoms designated numbers 1, 2 and 3, 4 in Fig. 2. This plot allows us to illustrate the position of the dislocation lines corresponding to the initial approximation of the isolated kink and its relaxed core structure (Fig. 3). The width of the single kink in TiAl predicted by our atomistic simulations is  $16b$ . This value is in good agreement with the continuum estimate of the width of the kink.

### 3.2. Kink-pair

The energy of two sharp kinks as a function of their separation  $L$  can be determined quite accurately when they are well separated [27]. The kink-pair can be regarded as being composed of straight line segments, and the energy is calcu-

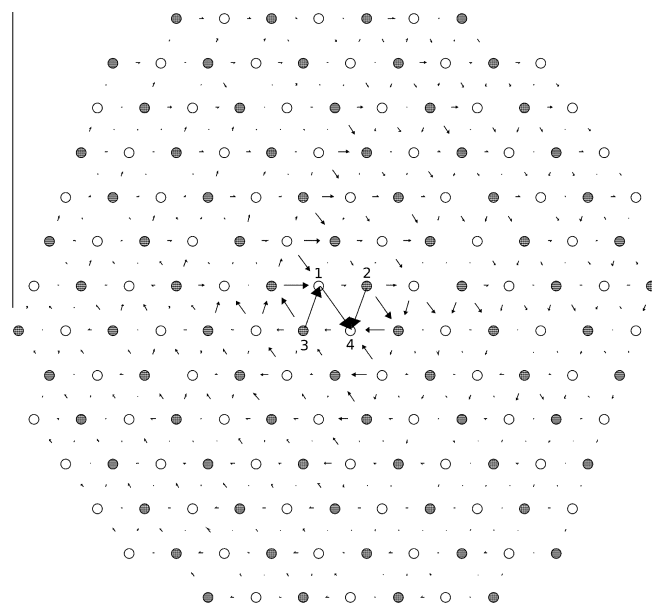


Fig. 2. Differential displacement plot showing the core structure of the central cell of the kinked dislocation line. The arrows are as in Fig. 1. This shows the plane of atoms perpendicular to the Burgers vector in the region separating two long screw dislocations having elastic centres displaced by the kink height,  $h$ . Hence a kink is lying along the  $[11\bar{2}]$  direction in the plane of the diagram. The core of the two  $\frac{1}{2}[1\bar{1}0]$  screw dislocations spreading onto two adjacent  $(111)$  and two adjacent  $(1\bar{1}1)$  planes can thereby be clearly seen.

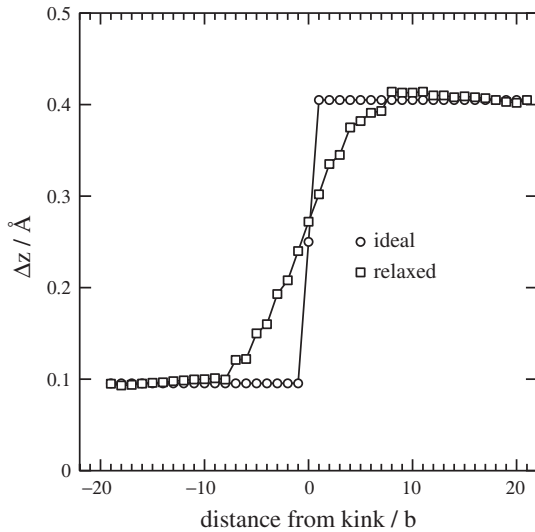


Fig. 3. Core spreading of an isolated kink. The relative displacement,  $\Delta z = [z_3 + z_4 - (z_1 + z_2)]/2$ , between the average  $z$ -coordinates of the atoms designated numbers 1, 2 and 3, 4 in Fig. 2 is plotted against distance from the kink centre in units of  $b$ . In the ideal, unrelaxed case this amounts to a “perfect” kink. The relaxed structure represents what in the text we refer to as an “oblique” kink, or non-pure edge kink. We see that the width of a relaxed kink is on the order of 10 Burgers vectors.

lated as the energy of the interactions between the line segments, including the self-interaction. The energy of two kinks can be separated into individual kink energies  $2E_k$  and interaction energy  $E_i$ .

$$E(L) = 2E_k + E_i$$

The energy of two mixed orientation, “oblique” kinks is expressed equivalently, provided that the kink-pair is separated by a distance  $L$  greater than the kink width  $w$ . When this condition does not hold,  $E(L)$  can no longer be separated into individual kink energies and interaction energy. The continuum estimation of the elastic energies of such configurations is difficult.

Applying the BOP-GFBC technique, we determine the core structure and energy of a kink-pair as a function of the distance between the kinks. The two relaxed configurations of the 2-D screw dislocation were used to obtain initial approximations to the structure of two pure edge kinks separated by distances from  $1b$  to  $23b$ . Core structures were relaxed to obtain the energy of the kink-pairs. The results are plotted in Fig. 4. The differences  $\Delta z$  between the average  $z$ -coordinates of atoms 1, 2 and 3, 4, which illustrate the shape of the dislocation lines for several kink-pairs, are shown in Fig. 5. The atomistic simulations predict that a screw segment of the dislocation line between both kinks transfers to the adjacent Peierls valley only if the distance between the kinks  $L$  is greater than the kink width (i.e.  $L > 16b$ ). The formation energy of two kinks in this case can be determined quite accurately by using non-singular continuum theory of dislocations [27]. By comparing the energies of two kinks separated by distances  $L > 16b$ , predicted by non-singular continuum theory, with the

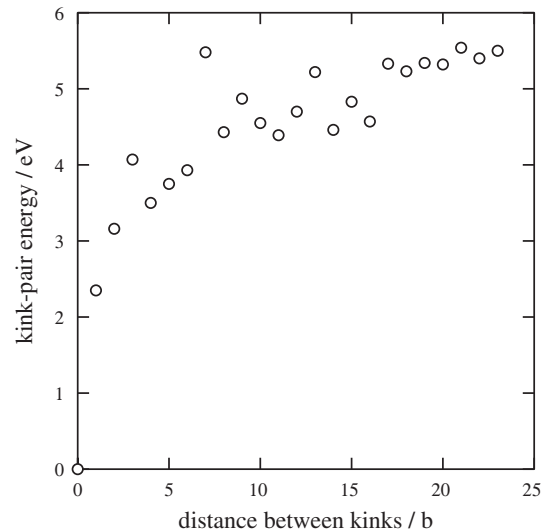


Fig. 4. Kink-pair formation energy as a function of the separation between the kinks. Here we constrain the kink-pair separation in the 3-D simulation as described in the text and show the energy of the corresponding relaxed kink-pair.

corresponding atomistic data, we can determine the spreading radius (see Section 2) or cut-off parameter. The value of the cut-off parameter obtained in this way is  $r_c = 0.125b$ .

We made continuum calculations of the formation energy both for pure edge, or “perfect”, and oblique kinks. In both cases we obtained similar results for the energy of the kinks. The relative discrepancy between the formation energies of perfect and oblique isolated kinks is 0.25. For kink-pairs separated by distance  $L > w$ , we find that the

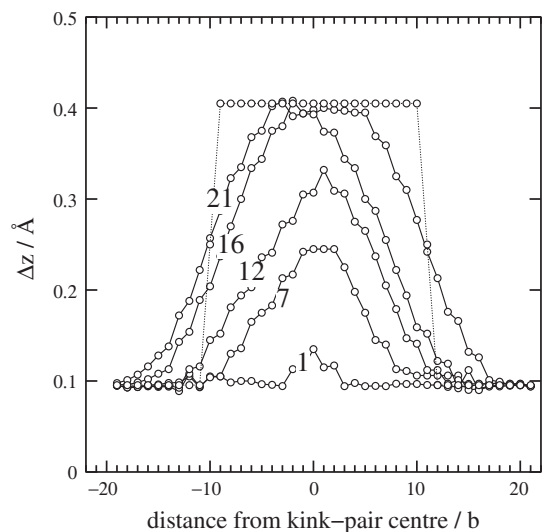


Fig. 5. The shape of the dislocation lines for kink-pairs with different distances  $w$  between the kinks. As in Fig. 3, we show the relative displacement,  $\Delta z$ , this time at the cores of a kink-pair, constrained as in Fig. 4 to a separation  $w/b$ , this being indicated on each set of data. The dotted line at  $w = 21b$  refers to an “ideal”, unrelaxed kink-pair. This illustrates the point we make in the text that for a kink-pair to be identifiable in a kMC simulation its separation must be greater than  $\sim 16b$ , so that it extends into the next Peierls valley.

relative discrepancies between the energies of perfect and oblique kinks is about 0.5. Taking into account these calculations, we approximate the real oblique kinks on ordinary screw dislocation in our kMC model by perfect edge segments. The approximation of perfect kinks is appropriate when the kink width is smaller than the distance between two kinks in a kink-pair. In this case, calculation within the non-singular continuum theory and perfect kinks approximation provides a correct result for the self-stress exerted on a dislocation segment.

### 3.3. Kink migration

In order to estimate the energy barrier for kink migration, we started with a simulation block containing the fully relaxed core structure of an isolated kink on an ordinary screw dislocation. To this we applied an incrementally increasing pure shear stress such that the force on the dislocation pushes the kink along the dislocation line. In practice, this stress is imposed by applying the appropriate homogeneous shear strain, which is evaluated with anisotropic elasticity theory. This strain was superimposed on the dislocation displacement field for all the atoms. Relaxation was carried out at every incremental step in the applied stress, until the kink migrates one crystal period along the dislocation line. At each step we calculated the change in the total energy of the cell as the kink migrates from its initial to final position. In particular, the maximum energy difference along the path is the energy barrier of migration of a single kink. Fig. 6 shows the energy of an isolated kink during its motion between two adjacent Peierls valleys. The energy is plotted at the nine incrementally increasing shear stresses that we have been working with. We obtain 0.13 eV for the energy of migration of a single kink on a screw ordinary dislocation in  $\gamma$ -TiAl.

In contrast to the high Peierls barrier for kink-pair nucleation ( $\sim 6$  eV, see Fig. 4), kink motion on the ordinary screw dislocation in TiAl should be very easy, as manifested in the low kink (or secondary) Peierls barrier. A high mobility of nucleated kinks should be expected, given that the applied stress in our simulations (rather less than the Peierls stress  $\sigma_P = 0.04C_{44}$ [20]) far exceeds the secondary Peierls stress ( $0.0023C_{44}$ ) determined in our atomistic simulations. The low energy barrier and secondary Peierls stress mean that kink migration along the ordinary screw dislocation is not thermally activated but is limited by phonon drag. Therefore, the kink velocity in the present kMC simulations is calculated as

$$v_k = \sigma_g \frac{b}{B}$$

where  $\sigma_g$  is the glide component of the resolved shear stress,  $b$  is the Burgers vector and  $B$  is the phonon drag coefficient. In our simulations we use the same numerical value of the drag coefficient for kink motion,  $B = 1.5 \times 10^{-5}$  Pa s, as in Fivel et al. [37].

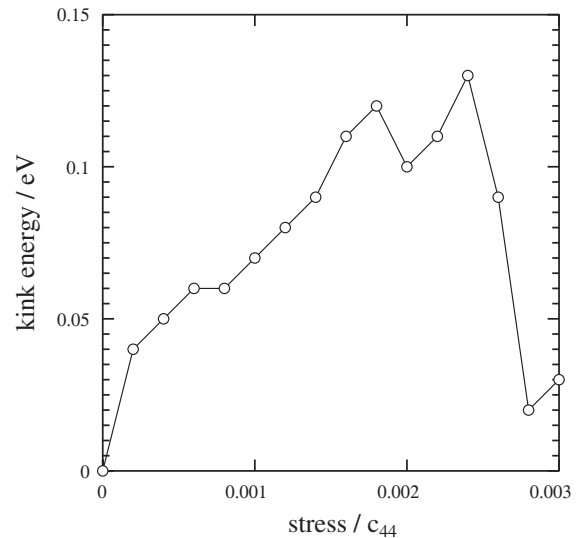


Fig. 6. The energy of an isolated kink during transition between two adjacent secondary Peierls valleys. The applied stress is in units of the shear elastic constant,  $c_{44}$ .

## 4. Results

In this section we present the results of kMC simulations of ordinary screw dislocation motion under  $0.75\sigma_P$  shear stress with different orientations of the maximal resolved shear stress (MRSS) plane. The total length of the S-segments are  $4000b \simeq 1.1 \mu\text{m}$  while each E-segment is only  $6.5 \text{ \AA}$ . Since the typical measured distance separating two pinning points is  $0.1\text{--}0.15 \mu\text{m}$  [13], the choice of this length of the dislocation line in our simulations is to maintain enough space for intrinsic pinning of the ordinary dislocation. Two different shear stress orientations of the MRSS plane have been tested in our kMC simulations: (i) single slip conditions and (ii) non-symmetrical double slip conditions, each of them at different temperatures between 600 and 1200 K. The choice of such a moderately high stress and temperature values in these simulations is to maintain a sufficient number of kinks on the dislocation. In the case of single slip conditions, the MRSS plane is parallel to the primary glide plane (111). The resolved shear stress on the primary glide plane is much larger than that in the secondary plane, and kink-pairs mostly nucleate on this plane. If the pinning points are supposed to be intrinsic, they are initiated by the collision of superkinks nucleated in both primary and cross-slip planes, and transformed into jogs by double cross-slip. In the case of non-symmetrical double slip conditions the MRSS plane bisects two glide planes (111) and ( $1\bar{1}1$ ), making kink-pair nucleation almost equally probable on both planes. We expect that collision of kinks nucleated in both primary and cross-slip planes, resulting in self-pinning, should be readily observed in this case.

However, for both the shear stress orientations of the MRSS plane the simulation results were very surprising, in

that there is always only one kink-pair along the entire dislocation line. Kink nucleation is rare and existing kinks tend to glide along the dislocation line through the periodic boundary conditions and recombine before the next kink nucleation event occurs. The averaged kink-pair nucleation rate per lattice site on the glide plane is  $J_{k-p} = 1.5 \times 10^5 b^{-1} s^{-1}$ , and the average kink velocity is  $v_k \approx 10^{14} b s^{-1}$ . The interplay between the rate of kink-pair nucleation and the kink migration velocity gives rise to a particular length scale  $L_c$  such that when a dislocation is shorter than  $L_c$  there is always only one kink-pair along the entire dislocation line. For typical kink-pair nucleation rate and kink migration velocity in our simulations, we find that this length scale is more than  $10 \mu\text{m}$ . Comparison with the typical observed distance separating two pinning points indicates that the probability for self-pinning and an intrinsic nature of the pinning points of screw ordinary dislocation in  $\gamma$ -TiAl is negligible.

In order to demonstrate self-pinning of the ordinary dislocation, we artificially reduced the kink migration velocity by increasing the phonon drag coefficient. With decreasing kink migration velocity, the number of kink-pairs nucleated on both glide planes along the dislocation line steadily increases. At  $B = 5 \times 10^{-3} \text{ Pa s}$ , corresponding to a kink migration velocity  $v_k \approx 3 \times 10^{11} b s^{-1}$ , a few pinning points are generated along the dislocation line, leading to cusp formation (see Fig. 7). The rate of self-pinning and cusp formation along the screw direction is higher in the case of non-symmetrical double slip conditions. The process of intrinsic pinning is initiated by collision of two kink-pairs formed in both primary and cross-slip planes. Such elementary jogs grow in size when more kinks pile up on either side of the initial pinning point, forming superjogs. The kinks in the pile-ups on two sides of the pinning point belong to different parallel primary glide planes. If the dislocation lines on two sides of the pinning point cross each other, they may reconnect by recombination of kink-pairs. As a result, the dislocation line is now reduced in size, leaving behind a prismatic loop, as shown in Fig. 7. The cusps are easily released by this unzipping mechanism and straight dislocations along the screw direction are restored.

The separation between the pinning point and the unzipping are functions of temperature and shear stress orientations of the MRSS plane. In the case of non-symmetrical double slip conditions, pinning, unzipping and formation of prismatic loops aligned along the screw direction are frequently observed in our kMC simulations. At lower temperatures and single slip conditions the rate of self-pinning and unzipping is less. Due to the lower unzipping rate, in this case we observed formation of dipoles as a result of propagation of screw dislocation line on both sides of the pinning points.

## 5. Discussion

The results of our simulations indicate that, in the unit processes of ordinary dislocation glide described by the kink-pair formation and migration model, nucleation of sustainable kink-pairs is rate limiting, and hence plays an important role in determining both the velocity of the dislocation and its glide mechanism.

The specific ordinary dislocation mechanisms expected in the  $L1_0$  structure were explored by Fivel et al. [37] through an adaptation of a 3-D mesoscopic dislocation simulation initially developed by Kubin et al. [38]. Using simple rules for kink-pair nucleation and propagation on ordinary screw dislocations, the simulation reproduced the main features of the “local pinning unzipping” mechanism [39] (pinning of cross-slip-generated jogs, cusp unzipping and formation of aligned prismatic loops). It was concluded that extrinsic obstacles do not seem to be necessary to account for both the observed microstructures and the stress anomaly [37]. This conclusion concerning the dislocation glide mechanism was a result of the high kink-pair nucleation rate employed by Fivel et al. [37]. The high probability of thermally activated kink-pair nucleation followed from the low kink-pair activation energy (0.45 eV) that they used. Since no experimental measurement of the activation energy is available owing to the stress anomaly, the activation energy in Ref. [37] is simply taken to be in the range of the analytically calculated activation enthalpy

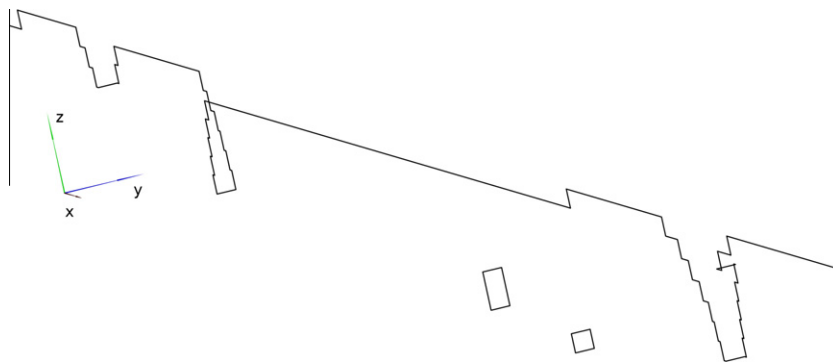


Fig. 7. A typical outcome of the kMC simulations, showing the cusped character of the dislocation line observed at reduced kink mobility. The MRSS plane bisects two glide planes  $(111)$  and  $(\bar{1}\bar{1}1)$  making kink-pair nucleation almost equally probable on both planes. The process of self-pinning is initiated by the collision of kinks nucleated in both primary and cross-slip planes. The cusps are released by recombination of the kink-pairs on both sides of a pinning point, leaving behind debris (prismatic loops).

for the cross-slipping back from the secondary  $(1\bar{1}1)$  cross-slip plane [9].

On the other hand, our atomistic simulations show that the kink-pair activation energy is one order of magnitude higher, which in its turn leads to a much lower thermally activated kink-pair nucleation rate. The interplay between the rate of kink-pair nucleation and the high kink migration velocity due to the low secondary Peierls barrier leads to a low density of kink-pairs in both  $\{111\}$  glide planes at length scales at which pinning of the dislocation line should be expected. In the absence of obstacles, kinks on the ordinary screw dislocation have very high mobilities, limited predominantly by lattice drag resistance. In the presence of solute atoms, the rate of kink migration is determined by the solute–kink interaction. The solute–dislocation interaction can be divided into two parts, depending on the distance of the solute from the dislocation segment: one associated with the long-range elastic fields of the solute and the other with the short-range solute–core interaction. If the solute is close to the dislocation core, the solute–core interaction provides a barrier  $E_b$  to the motion of the kink. Usually kinks require thermal activation to overcome the local energy barrier  $E_b$  associated with solute atoms near the core. In this case, the rate of kink migration is determined by the magnitude of the solute–kink interaction energy  $E_b$ .

Owing to the high kink-pair activation energy and high kink mobility in the absence of interaction with extrinsic obstacles predicted by the present atomistic simulations, the probability for self-pinning is negligible, and therefore the nature of the pinning points on screw ordinary dislocations in pure  $L1_0$  crystal cannot be intrinsic. It follows that the observed dislocation pinning must be attributable to extrinsic obstacles. These obstacles presumably reduce kink migration velocity, thus increasing the density of kink-pairs in both  $\{111\}$  glide planes at length scales at which pinning of the dislocation line should be expected. The increased density of kink-pairs formed in both primary and cross-slip planes leads to a higher probability of collision between two kinks and the formation of jogs.

The results of our simulations indicate that the pinning of screw ordinary dislocations can be attributed to the relation between extrinsic obstacles and extensive cross-slip. As shown in the present study, the lateral propagation of kinks occurs very quickly, and this implies a very small probability of movements in the adjacent slip plane of the screw segments which are lying in the sessile configuration before this lateral propagation. If a part of a dislocation moving without any interaction with extrinsic obstacles makes a double cross-slip, the whole dislocation moves onto a primary glide plane parallel to the initial one since no obstacles oppose the lateral propagation of the edge segments lying in the cross-slip plane. If the dislocation moves in a crystal containing extrinsic obstacles, the number of kink-pairs nucleated on both primary and cross-slip planes along the dislocation line steadily increases as a result of the reduced mobility of kinks due to the solute–dislocation interaction. The increased density of kink-pairs nucleated

in both glide planes leads to a higher probability of collision between two kinks and the formation of jogs by double cross-slip. The pinning points and dipoles dragged by screw dislocations are thus probably formed through this combination of extrinsic obstacles and cross-slip in a crystal containing impurities.

## 6. Conclusions

In our kMC simulations of ordinary dislocation mobility in TiAl we examined an isolated dislocation moving at applied stress by the kink propagation mechanism through adjacent Peierls valleys in the  $L1_0$  crystal structure of  $\gamma$ -TiAl. The rates of kink nucleation and migration events were expressed in terms of their respective energy barriers, which were computed using fully three-dimensional atomistic simulations employing Green's function boundary conditions and a quantum mechanical prescription for the interatomic forces. The results of the present simulations indicate that the interplay between the rate of kink-pair nucleation and the kink migration velocity leads to a surprisingly low density of kink-pairs in both glide planes at length scales at which intrinsic pinning of the dislocation line should be expected. Therefore, the probability of intrinsic pinning, which is initiated by the collision of kinks nucleated in both primary and cross-slip planes and transformed into jogs by double cross-slip, is negligible.

If we artificially reduce the kink migration velocity, the number of kink-pairs nucleated on both glide planes along the dislocation line steadily increases. The increased density of kink-pairs formed in both primary and cross-slip planes leads to a higher probability of collision between two kinks and the formation of jogs, demonstrating that our method is capable of producing the intrinsic self-pinning, albeit at unphysical values of the parameters.

We conclude that the pinning points are not intrinsic in nature. The pinning of ordinary dislocations and anomalous mechanical behaviour in  $\gamma$ -TiAl must therefore be correlated to extrinsic obstacles. Amongst the other possible mechanisms, obstacles could reduce kink migration velocity, thus increasing the density of kink-pairs in both glide planes at length scales at which pinning of the dislocation line should be expected.

## Acknowledgement

This research was supported by the EPSRC, under Grant No. EP/E025854/1.

## References

- [1] Appel F, Wagner R. Mater Sci Eng 1998;R22:187–268.
- [2] Gregori F, 1999, PhD thesis, Université de Paris VI.
- [3] Viguier B, Hemker KJ, Bonneville J, Louchet F, Martin JL. Philos Mag A 1995;71:1295–312.
- [4] Sriram S, Dimiduk DM, Hazzledine P, Vasudevan VK. Philos Mag A 1997;76:965–93.
- [5] Couret A. Philos Mag A 1999;79:1977–94.

- [6] Inui H, Matsumuro M, Wu DH, Yamaguchi M. *Philos Mag A* 1997;75:395–423.
- [7] Nakano T, Hagihara K, Seno T, Sumida N, Yamamoto M, Umakoshi Y. *Philos Mag Lett* 1998;78:385–91.
- [8] Louchet F, Viguier B. *Philos Mag A* 1995;71:1313–33.
- [9] Louchet F, Viguier B. *Philos Mag A* 2000;80:765–79.
- [10] Messerschmidt U, Bartsch M, Haussler D, Aindow M, Hattenhauer R, Jones IP. *Mater Res Soc Symp Proc* 1995;364:47–52.
- [11] Haussler D, Bartsch M, Jones IP, Messerschmidt U. *Philos Mag A* 1999;79:1045–71.
- [12] Gregori F, Veyssère P. *Philos Mag A* 2000;80:2913–33.
- [13] Couret A. *Intermetallics* 2001;9:899–906.
- [14] Zghal S, Menand A, Couret A. *Acta Metall Mater* 1998;46:5899–905.
- [15] Morris MA. *Intermetallics* 1996;4:417–26.
- [16] Katzarov IH, Cawkwell MJ, Paxton AT, Finnis MW. *Philos Mag* 2007;87:1795–809.
- [17] Katzarov IH, Paxton AT. *Philos Mag* 2009;89:1731–50.
- [18] Katzarov IH, Paxton AT. *Acta Mater* 2009;57:3349–66.
- [19] Katzarov IH, Paxton AT. *Phys Rev Lett* 2010;104:225502.
- [20] Porizek R, Znam S, Nguyen-Manh D, Vitek V, Pettifor DG. *Mater Res Soc Symp Proc* 2003;753:BB4–6.
- [21] Bulatov V et al. *Nature* 1998;301:669–72.
- [22] Tang M, Kubin LP, Canova GR. *Acta Mater* 1998;9:3221–35.
- [23] Cai W, Bulatov VV, Justo JF, Yip S, Argon AS. *Phys Rev Lett* 2000;84:3346–9.
- [24] Cai W, Bulatov VV, Yip S. *J Comput Aided Mater Des* 1999;6:175–83.
- [25] Deo CS, Srolovitz DJ, Cai W, Bulatov VV. *J Mech Phys Solids* 2005;53:122347.
- [26] Cai W, Bulatov VV, Yip S, Argon AS. *Mater Sci Eng A* 2001;309–310:270–3.
- [27] Hirth JP, Lothe J. *Theory of dislocations*. 2nd ed. New York: Wiley-Interscience; 1982.
- [28] Cai W, Arsenlis A, Weinberger C, Bulatov V. *J Mech Phys Solids* 2006;54:561–87.
- [29] Deo CS, Srolovitz DJ. *Phys Rev B* 2001;63:165411.
- [30] Bulatov VV, Cai W. *Computer simulations of dislocations*. Oxford: Oxford University Press; 2006.
- [31] Pettifor DG. *Phys Rev Lett* 1989;63:2480–3.
- [32] Pettifor DG, Aoki M. *Philos Trans Roy Soc Lond Ser A – Math Phys Eng Sci* 1991;334:439–49.
- [33] Znam S, Nguyen-Manh D, Pettifor DG, Vitek V. *Philos Mag A* 2003;83:415–38.
- [34] Sinclair JE. *J Appl Phys* 1971;42:5321–9.
- [35] Rao S, Hernandez C, Simmons JP, Parthasarathy TA, Woodward C. *Philos Mag A* 1998;77:231–56.
- [36] Petukhov BV. *Phys. Metals Metallogr. (USSR)* 1983;56:123–9.
- [37] Fivel MC, Louchet F, Viguier B, Verdier M. *Mater Res Soc Symp Proc* 2001;646. N7.10.1–10.6.
- [38] Kubin LP, Canova GR, Condat M, Devincre B, Pontikis V, Bréchet Y. *Solid State Phenom* 1992;23/24:455–72.
- [39] Louchet F, Viguier B. *Scripta Metall* 1994;31:369–74.